Roles of Curvature and Hydrophobic Interstice Energy in Fusion: Studies of Lipid Perturbant Effects†

Md. Emdadul Haque and Barry R. Lentz*

Department of Biochemistry and Biophysics and Program in Molecular & Cellular Biophysics, CB #7260, University of North Carolina at Chapel Hill, North Carolina 27599-7260

Received October 3, 2003; Revised Manuscript Received January 2, 2004

ABSTRACT: We have examined the effects of small amounts (1−4 mol %) of lipids of different molecular shapes, long chain lipids, and hydrocarbon on the kinetics of PEG-mediated fusion of 1,2-dioleoyl-3-sn-phosphatidylcholine/1,2-dioleoyl-3-sn-phosphatidylethanolamine/sphingomyelin/cholesterol (DOPC/DOPE/SM/CH, 35:30:15:30) sonicated vesicles. The effects of these lipid perturbants were different for different steps in the fusion process and varied with the ratio of the cross-sectional areas of headgroup to acyl chain moieties. For lipids with a ratio <1 (negative intrinsic curvature), a decrease in this ratio led to a dramatic increase in the initial rate of vesicle contents mixing but left the initial rate of lipid mixing roughly unchanged. For lipids with ratios >1 (positive intrinsic curvature), the initial rates of both lipid and contents mixing decreased mildly with increasing ratio. In the context of the "stalk model" for fusion, lipid mixing reflects mainly formation of the initial fusion intermediate (stalk), while contents mixing reflects conversion of this intermediate either to a second intermediate or to a fusion pore. Results with positively curved lipids (ganglioside, GM1; lysophosphatidylcholine, LPCs) and negatively curved lipids (dioleoylglycerol, DOG, and 1,2-diphytanoyl-sn-glyvero-3-phosphatidylcholine, DPhPC) can be taken as supportive of the usual interpretation of the stalk model in terms of bending energy, but enhancement of fusion in the presence of long-chain phospholipids, hexadecane, as well as a mixture of GM1 plus hexadecane could not be explained by their curvature alone. We propose that the ability of a lipid perturbant to compensate for lipid packing mismatch, that is, to lower "void" energy, must be taken into account, along with intrinsic curvature, to explain the ability of lipid perturbants to promote pore formation.

Membrane fusion is at the heart of eukaryotic cell life. Carefully regulated membrane fusion is required for cell compartmentalization, for the import of large molecules into the cell, and for the export of both waste and signaling molecules. Studies of the molecular mechanism of membrane fusion in simple model systems provide fundamental insights into the fusion process in biomembranes in which complex protein machines manipulate lipid bilayers to promote the lipid molecule rearrangements required for fusion. Such mechanistic studies have evolved a fairly widely accepted model for this process that derives from the original proposal that two bilayers brought into close contact can merge their contacting (cis) monolayers in a toroidal "stalk" that joins the contacting external monolayers of the two original bilayers (*1*, *2*). This hypothesis has been extended to a more detailed "stalk hypothesis" that envisions how this initial stalk contact might evolve into a fusion pore (*3*−*7*). It has also been suggested that fusion proteins might have the job of bringing membranes into contact and bending them so that they form a stalk (*8*) and then perhaps of promoting the subsequent evolution of the stalk to a later intermediate (*9*). While the occurrence of an initial stalk contact is widely accepted, there are alternative mechanisms that have been proposed to explain how this structure might evolve to a pore, especially during protein-mediated fusion (*10*, *11*).

Since the intermediate lipidic structures on the path to pore formation are predicted by the stalk hypothesis to be highly curved, efforts to test this hypothesis have examined the effects of differently shaped lipids such as lysophosphatidylcholine (LPC[1]) on the extent of model membrane, microsomal membrane, exocytotic, and viral fusion. LPC added to the medium between fusing membranes inhibited both hemifusion (merging of contacting leaflets presumably

† Supported by USPHS Grant GM32707 to B.R.L.

* To whom correspondence should be addressed. Tel: 919-966-5384. Fax: 919-966-2852. E-mail: uncbrl@med.unc.edu.

[1] Abbreviations: SUVs, small unilamellar vesicles; QELS, quasi-elastic light scattering; DOPC, 1,2-dioleoyl-3-*sn*-phosphatidylcholine; DOPE, 1,2-dioleoyl-3-*sn*-phosphatidylethanolamine; DOPS, 1,2-dioleoyl-3-*sn*-phosphatidylserine; SM, sphingomyelin (bovine brain); CH, cholesterol; GM1, ganglioside (ovine brain); DOG, dioleoylglycerol; DPhPC, 1,2-diphytanoyl-3-*sn*-phosphatidylcholine; DiPoPE, 1,2-dipalmitoleoyl-3-*sn*-phosphoethanolamine; DNPC (C24), 1,2-dinervonoyl-3-*sn*-phosphatidylcholine; DEPC (C22), 1,2-dierucoyl-3-*sn*-phosphatidylcholine; LPC24, 1-lignoceroyl-2-hydroxy-3-*sn*-phosphocholine; LPC16, 1-palmitoyl-2-hydroxy-3-*sn*-phosphocholine; LPC, lysophosphatidylcholine; BODIPY530/550 C_{12}-HPE, 2-(4,4-difluoro-5,7-diphenyl-4-bora-3a,4a-diaza-*s*-indacene-3-dodecanoyl)-1-hexadecanoyl-*sn*-glycero-3-phosphoethanolamine; β-BODIPY500/510 C_{12}-HPC, 2-(4,4-difluoro-5,7-diphenyl-4-bora-3a,4a-diaza-*s*-indacene-3-dodecanoyl)-1-hexadecanoyl-*sn*-glycero-3-phosphocholine; $C_{12}E_8$, dodecyloctaethylene glycol monoether; DPH, 1,6-diphenyl-1,3,5-hexatriene; TMA-DPH, 1-[4-(trimethylammonium)-6-phenyl]-1,3,5-hexatriene; Tb^{3+}, terbium chloride; DPA, pyridine-2,6-dicarboxylic acid; TES, *N*-[tris(hydroxymethyl)methyl]2-2-aminoethane sulfonic acid; PEG, poly(ethylene glycol).

10.1021/bi035794j CCC: $27.50
Published on Web 03/04/2004

to form a stalk; generally marked by mixing of lipids) and full fusion (generally marked by mixing of trapped contents) (*5*, *12*−*15*). This was interpreted as being due to the positive intrinsic curvature of LPC destabilizing the negatively curved leaflets of the stalk intermediate and thus was taken as supporting the stalk hypothesis. However, arachidonic acid, which has the opposite intrinsic curvature of LPC, curiously had little effect on either hemifusion or fusion (*5*), although such negatively curved lipids are reported to increase both the rate and extent of fusion between hemagglutinin-expressing cells when added at much higher concentrations than those required to see an effect of LPC (*16*). Other studies with liposomes having an asymmetric distribution of LPC suggested that LPC might inhibit fusion by stabilizing the initial unfused state rather than by raising the free energy of the stalk intermediate (*17*, *18*). Martin et al. (*19*) and Pecheur et al. (*20*) have also suggested that inhibition by LPC of simian immune deficiency virus or influenza virus fusion might be due to a totally different mechanism, that is, to changes in the orientation or secondary structure or both of a portion of the protein fusion machines known as fusion peptide. Thus, although studies with LPC might offer support for the stalk hypothesis, significant unanswered questions remain about how lipid perturbants with different molecular shapes might alter fusion. This is especially true because intrinsic curvature reflects ratios of molecular areas in different regions of the bilayer and does not take into account the volume of the molecule in different regions of the bilayer.

In the present study, we used a very simple pure lipid model system in which PEG aggregates vesicles (but does not interact directly with them) (*21*) and creates a compressive osmotic stress that favors fusion (*22*). While the compressive osmotic stress favors fusion, it is not required, since PEG-induced aggregation of fusogenic vesicles causes fusion even in the absence of an osmotic gradient (*22*). Very small amounts of a variety of perturbant amphipaths were incorporated into a lipid mixture that we showed to be optimal for fusion (*23*). We recorded the influences of these perturbants on the kinetics of both lipid mixing and contents mixing induced by PEG. We have used this system to ask two questions: (1) can we explain the effects of amphipathic lipid impurities in terms of only their intrinsic curvatures and (2) do perturbants have different effects on different stages of the fusion process?

MATERIALS AND METHODS

Materials. 1,2-Dioleoyl-3-*sn*-phosphatidylcholine (DOPC[1]), 1,2-dioleoyl-3-*sn*-phosphatidylethanolamine (DOPE[1]), sphingomyelin (bovine brain, SM[1]), ganglioside (ovine brain, GM1[1]), 1,2-dinervonoyl-3-*sn*-phosphotidylcholine (DNPC[1]), 1,2-dierucoyl-3-*sn*-phosphotidylcholine (DEPC[1]), 1-lignoceroyl-2-hydroxy-3-*sn*-phosphocholine (LPC24[1]) and 1-palmitoyl-2-hydroxy-3-*sn*-phosphocholine (LPC16[1]), 1,2-diphytanoyl-3-*sn*-phosphatidylcholine (DPhPC[1]), and 1,2-dipalmitoleoyl-3-*sn*-phosphoethanolamine (DiPoPE[1]) were purchased from Avanti Polar Lipids, Inc. (Birmingham, AL) and used without further purification. 1-Oleoyl-2-acetyl-*sn*-glycerol (DOG[1]) was purchased from Sigma Chemical Company (St. Louis, MO). Space filling models of these compounds that illustrate their molecular shapes are shown in Figure 1. Concentrations of all lipid stock in chloroform

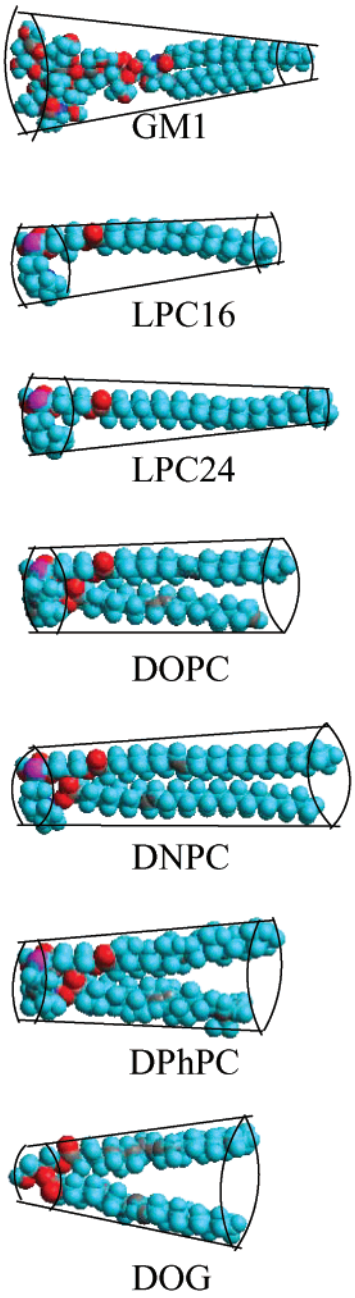

FIGURE 1: Space filling models (Chem 3D software, Cambridge Soft, Cambridge, MA) of the lipid perturbants considered here. Atom code: hydrogen (light blue), oxygen (red), nitrogen (dark blue), and carbon (black). Lipid shapes (based on head and tail group cross-sectional area) are illustrated by truncated cones encompassing each molecule.

were determined by phosphate assay (*24*). Cholesterol (CH[1]) was purchased from Avanti Polar Lipids and was further purified as previously reported (*25*). 2-(4,4-Difluoro-5,7-diphenyl-4-bora-3a,4a-diaza-*s*-indacene-3-dodecanoyl)-1-hexadecanoyl-*sn*-glycero-3-phosphoethanolamine (*β*-BODIPY530/550 C_{12}-HPE[1]), 2-(4,4-difluoro-5,7-diphenyl-4-bora-3a,4a-diaza-*s*-indacene-3-dodecanoyl)-1-hexadecanoyl-*sn*-glycero-3-phosphocholine (*β*-BODIPY500/510 C_{12}-HPC[1]), 1,6-diphenyl-1,3,5-hexatriene (DPH[1]), and 1-[4 (trimethylammonium)-6-phenyl]-1,3,5-hexatriene (TMA-DPH[1]) were purchased from Molecular Probes (Eugene, OR). Terbium (Tb^{3+}) chloride was purchased from Johnson Matthey Co. (Ward Hill, MA). Dipicolinic acid (DPA[1]), *N*-[tris(hy-

droxymethyl)methyl]2-2-aminoethane sulfonic acid (TES[1]), and hexadecane were purchased from Sigma Chemical Co. (St. Louis, MO). Poly(ethylene glycol) of molecular weight 7000−9000 (PEG[1] 8000) was purchased from Fisher Scientific (Fairlane, NJ) and further purified as previously reported (*26*). Dodecyloctaethylene glycol monoether ($C_{12}E_8$[1]) was purchased from Calbiochem (La Jolla, CA). All other reagents were of the highest purity grade available.

Vesicle Preparation. A stock solution of DOPC, DOPE, SM, and CH in a molar ratio of 33:30:15:20 was prepared in chloroform, and small amounts of perturbant lipid were mixed with aliquots from this stock in chloroform and were dried under nitrogen. The dried mixed lipids were converted to small unilamellar vesicles (SUVs) using a Sonicator 3000 (Misonix, Farmingdale, NY) at a power setting 9−12 W with a titanium flat probe tip as described earlier (*23*). SUVs were prepared with 750 mM NaCl, 8 mM $TbCl_3$, 60 mM sodium citrate, and 10 mM TES for contents mixing, 750 mM NaCl, 80 mM DPA, and 10 mM TES for leakage, and 850 mM NaCl, 10 mM TES, 1mM $CaCl_2$, and 1 mM EDTA for lipid mixing, but assays (column buffer) were performed at 800 mM NaCl, 10 mM TES, 1 mM EDTA, and 1 mM $CaCl_2$ along with 5% PEG to balance internal osmotic strength between the external and internal vesicle compartments. Vesicle diameters were measured by quasi-elastic light scattering (QELS[1]) (*26*) to be 26−28 nm in all cases.

Contents Mixing and Leakage. Contents mixing and leakage were followed using the Tb/DPA contents mixing and leakage assays based on those originally proposed by Wilschut et al. (*27*) and adapted to monitor PEG-induced fusion under isoosmotic conditions (*22*). Lipid concentrations in all experiments were 0.2 mM.

Lipid Mixing Assay. Chain-labeled fluorescent lipid probes, BODIPY500-PC and BODIPY530-PE, in a 1:1 molar ratio were used as described previously for measuring lipid mixing during PEG-mediated vesicle fusion (*28*). Probe-containing vesicles were mixed with probe-free vesicles at a ratio of 1:4, and it was assumed that 100% lipid mixing corresponded to a 5-fold dilution of the probe.

DPH and TMA-DPH Fluorescence Anisotropy. A small volume (0.04−0.08% of vesicle sample volumes) of a stock solution of either DPH or TMA-DPH in methanol was added to PC/PE/SM/CH SUVs to achieve a final lipid/probe ratio of 200:1. The vesicles and probes were thoroughly mixed and incubated for 45 min until the fluorescence intensity saturated. An excitation wavelength of 360 nm was used with excitation slits of 4 and 4 nm, and a 450 nm cutoff filter was used in the emission in the T-format.

Differential Scanning Calorimetry. Experiments were carried out in a Microcal (Northampton, MA) VP isothermal calorimeter located in UNC's Macromolecular Interaction Facility. Samples (DiPoPE and 2 mol % perturbant lipids) were dispersed in TES buffer (100 mM NaCl and 10 mM TES) at a concentration of 5 mg/mL to measure the $L_\alpha-H_{II}$ phase transition temperature. The lamellar order-to-disorder phase transition of PC/PE/SM/CH multilamellar vesicles was also examined to check for the effect of GM1 on the PC/PE/SM/CH lamellar phase. Samples (1 mL) were degassed under reduced pressure for 30 min before being loaded into the calorimeter cell with a Hamilton gastight syringe. The scan rate for all experiments was 30 °C/h, and scans were performed between 20 and 60 °C. The thermograms (excess heat capacity vs temperature) were collected and analyzed with Origin (Microcal Software, Inc., Northampton, MA).

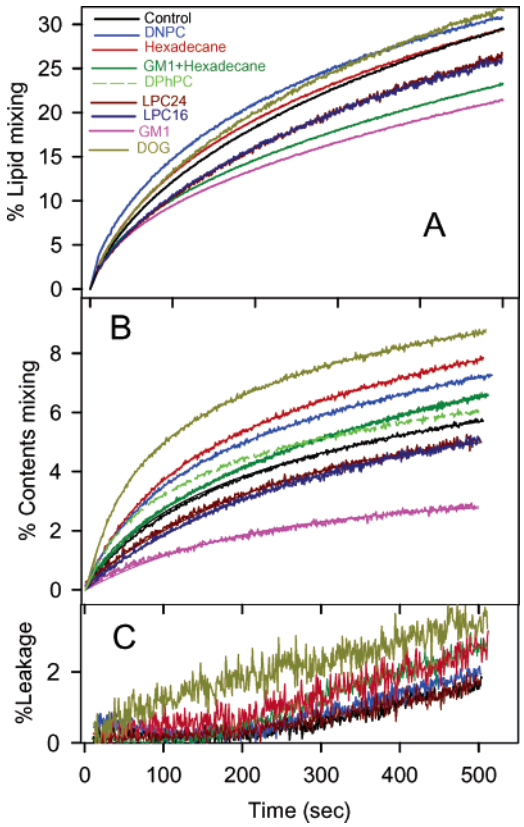

FIGURE 2: Effect of 2 mol % of different shaped lipids on time courses of (A) lipid mixing, (B) contents mixing, and (C) leakage in PC/PE/SM/CH (35:30:15:20 mol ratio) SUVs in the presence of 5% PEG, 10 mM TES, 800 mM NaCl, 1 mM EDTA, and 1 mM $CaCl_2$ and at 23 °C, pH 7.4. Data for control vesicles (black) and vesicles with 2 mol % of DOPC replaced with 2 mol % of various perturbants (color code shown in frame A) are shown. The time courses were fit to single and double exponentials as described in the legend to Table 1, with the results summarized in that table. Errors in the exponential constants of lipid mixing and contents mixing from repeats with a single vesicle preparation were 5−8%.

Measurements of Interlamellar Repeat Distances. Lamellar repeat periods for control and perturbant-containing (2 mol %) multilamellar vesicles at 5% PEG were determined by X-ray diffraction measurements, with the help of Dr. Tom McIntosh (Duke University), in the high-salt buffer used here, as described previously for a low-salt buffer (*23*).

RESULTS AND DISCUSSION

Perturbant Effects on Lipid Mixing Kinetics. Lipid mixing between juxtaposed vesicles should depend both on the probability or rate of formation of productive contacts (i.e., hemifused contacts) between vesicles and on the rate of lipid diffusion through these contacts. Because lipid lateral diffusion is orders of magnitude faster than the lipid mixing process that we measure, we take the position that lipid mixing reflects primarily the rate of formation of the initial fusion intermediate. Time courses of lipid mixing at 23 °C and 5 wt % PEG for DOPC/DOPE/SM/CH (35:30:15:20 mol ratio) control vesicles and for vesicles containing different perturbants are plotted in Figure 2A. Vesicles for these time courses contained 2 mol % perturbant lipid replacing 2 mol % DOPC. In the case of hexadecane, no compensation in

Table 1: Summary of Exponential Analysis of Contents and Lipid Mixing Data for 2 mol % Perturbants at 5% PEG[a]

Contents Mixing

perturbants	C_1	$k_1 \times 10^{-3}$	C_2	$k_2 \times 10^{-4}$	$C_1 + C_2$	IR[b] (%/s)
control			5.8 ± 0.02	55.3 ± 0.5	5.86	0.032
DOG	3.5 ± 0.06	24.7 ± 0.7	6.4 ± 0.03	34.0 ± 0.9	9.90	0.107
DPhPC	2.2 ± 0.06	22.6 ± 0.9	5.0 ± 0.02	30.6 ± 1.1	7.2	0.065
DEPC	2.7 ± 0.4	12.1 ± 1.3	6.0 ± 0.3	19.3 ± 5.0	8.66	0.044
DNPC	2.8 ± 0.1	15.4 ± 0.6	7.1 ± 0.2	18.3 ± 1.4	9.91	0.056
hexadecane	2.7 ± 0.1	15.8 ± 0.8	7.5 ± 0.1	22.1 ± 1.6	10.20	0.058
GM1			3.1 ± 0.02	37.1 ± 0.8	3.10	0.014
LPC24			5.6 ± 0.1	37.7 ± 0.6	5.57	0.021
LPC16			5.6 ± 0.1	36.0 ± 0.5	5.60	0.020
GM1 (2 mol %) + hex (1 mol %)	2.0 ± 0.3	12.8 ± 1.4	7.2 ± 0.4	17.9 ± 3.7	9.62	0.043
GM1 (2 mol %) + hex (2 mol %)	1.3 ± 0.1	20.6 ± 1.1	7.7 ± 0.1	22.0 ± 0.7	9.00	0.043

Lipid Mixing

perturbants	C_1	$k_1 \times 10^{-3}$	C_2	$k_2 \times 10^{-4}$	$C_1 + C_2$	IR[b] (%/s)
control	5.1 ± 0.1	24.8 ± 1.1	33.7 ± 0.1	25.4 ± 0.5	38.86	0.21
DOG	5.9 ± 0.16	21.6 ± 0.4	35.2 ± 0.2	23.2 ± 0.4	41.1	0.21
DPhPC	5.4 ± 0.1	22.5 ± 0.6	34.6 ± 0.1	21.9 ± 0.3	40.0	0.20
DNPC	6.3 ± 0.1	23.7 ± 0.7	31.5 ± 0.1	26.3 ± 0.4	37.85	0.23
hexadecane	6.5 ± 0.1	20.6 ± 3.4	32.0 ± 0.1	23.6 ± 0.3	38.56	0.21
GM1	3.7 ± 0.1	26.0 ± 1.3	24.8 ± 0.2	21.8 ± 2.9	28.50	0.15
LPC16	3.61 ± 0.1	27.6 ± 2.1	29.9 ± 0.2	23.4 ± 0.6	33.32	0.17
LPC24	3.56 ± 0.2	27.2 ± 2.0	33.5 ± 0.3	21.8 ± 0.6	37.00	0.17
GM1 + hex	4.81 ± 0.1	25.2 ± 0.4	26.8 ± 0.2	18.0 ± 0.3	31.62	0.17

[a] Time courses were fit to single [$f = C(1 - e^{-kt})$] and double [$f = C_1(1 - e^{-k_1 t}) + C_2(1 - e^{-k_2 t})$] exponential curves using Sigma Plot 2000 (SPSS Inc, IL), leading to initial rates (IR) of Ck and $C_1k_1 + C_2k_2$, respectively. Parameter uncertainties derived from the nonlinear least-squares procedures are indicated. [b] Initial rate.

the DOPC content was made, and concentrations of hexadecane are given as mole percent of total lipid with hexadecane not being counted as a lipid. These results clearly show how different lipid shapes had very different influences on the rate and extent of lipid transfer (Figure 2A) when vesicles are brought into close contact by PEG. Time courses were fit to double exponentials to obtain exponential constants,[2] preexponential factors, and initial rates, which are given in Table 1. Hexadecane (red), DOG (deep yellow), and DNPC (blue) had no effect on the rate of lipid mixing (within experimental error). This effect was confirmed by doing the experiments at different concentrations, as reported in Figure 3 for hexadecane (squares), DOG (hexagons), and DNPC (triangles). It is clear that none had a significant effect on the initial rate of lipid mixing within experimental error (Figure 3A). The extent of lipid mixing was also not affected significantly by these perturbants (Figure 3B) except that vesicles containing 4% DOG were not sufficiently stable to perform experiments, so no point is shown for DOG at this concentration.

Unlike the negatively curved lipids DOG and DPhPC (not shown in Figure 3), all positively curved lipids (GM1, LPC24, and LPC16) inhibited lipid mixing, although the effect of GM1 (purple) was much greater than that of LPC16 (dark blue) or LPC24 (reddish brown) (Figure 2A). Figure 3 sheds more light on the distinct effect of GM1. While all three positively curved lipids had a similar effect on the initial rate (Figure 3A), only GM1 (circles) dramatically decreased the extent of lipid mixing (Figure 3B). Since the extent of lipid mixing reflects the size of PEG-induced aggregates (*29*, *30*), this means that only GM1 measurably reduced aggregate size, probably due to the size or charge of its headgroup or both. Consistent with this interpretation, the two preexponential constants of the GM1 lipid mixing time course decreased in magnitude to the same extent with an increase in GM1 content (circles in Figure 3B inset), while the fast (open symbols) and slow (closed symbols) components of lipid mixing in the presence of LPC16 or LPC24 varied differently with increasing concentrations of these components (LPC16 shown as inverted triangles in Figure 3 inset). This suggests that there is a common mechanism at work in decreasing the extent of both components of the GM1 effect to such a large extent and that this mechanism does not contribute to decreasing the rate of the slow component for LPC16 and LPC24.

GM1 is a negatively charged lipid. Thus, its charge, in addition to its large headgroup, might account for its inhibitory effect. To separate the effects of charge and headgroup size, we compared the effects of DOPS and GM1 at a low ionic strength (100 mM NaCl) to their effects at a high ionic strength (800 mM NaCl). In low-salt buffer, both lipids inhibited lipid mixing and contents mixing, while in high-salt buffer, DOPS had no effect (data not shown). For this reason, all the experiments reported here were performed in high-ionic strength buffer (Materials and Methods), where these results suggest that the inhibitory effect of GM1 is due to its molecular shape (i.e., the size of its headgroup) and not to its charge.

Perturbant Effects on Contents-Mixing Kinetics. Since fusion seems to proceed in our model system through at least two semistable intermediate structures (*6*, *31*), the rate of contents mixing reflects several processes: (1) the rate of initial intermediate formation, (2) rate of conversion of initial to later intermediate, (3) rate of conversion of later intermediate to a pore, and (4) rate of diffusion of trapped contents through this pore. Lipid mixing provides information

[2] We will refer to these constants as "rate constants" k_1 and k_2 although they do not actually refer to rates, since we have not identified a kinetic model to which we are fitting our data, only a double exponential expression.

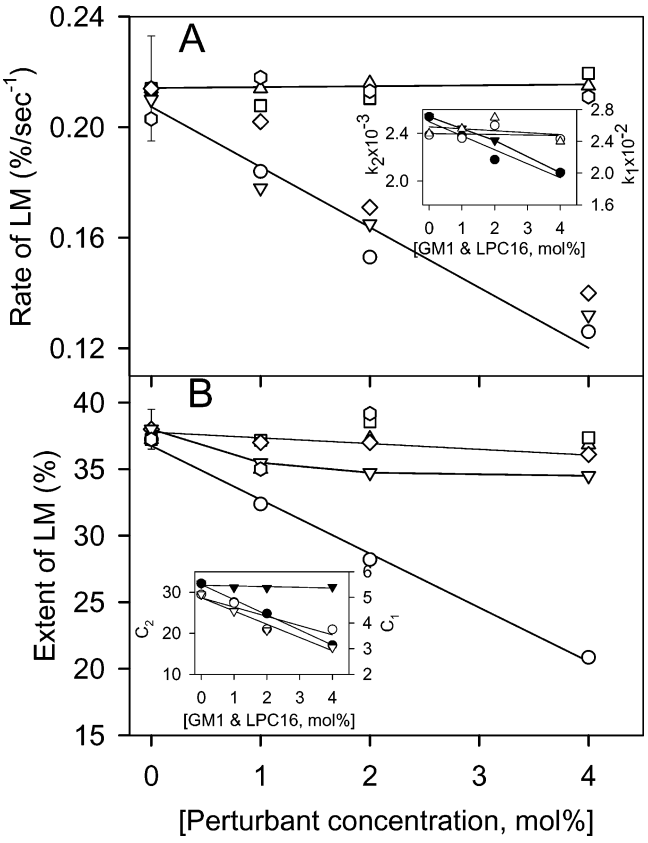

FIGURE 3: Effect of perturbant concentration on the initial rate (A) and extent (B) of PEG-mediated lipid mixing from time courses such as those shown in Figure 2. Data for GM1 (○), LPC24 (◇), LPC16 (▽), DNPC (△), DOG (⬡) and hexadecane (□) are shown. The inset to frame A shows k_1 (open symbols) and k_2 (closed symbols) for lipid mixing in the presence of GM1 and LPC16. The inset to frame B shows the preexponential factors, C_1 (open) and C_2 (closed). Experimental error bars in all experiments are very similar. We have shown error bar for control vesicles (PC/PE/SM/CH).

mainly about the first process, since the diffusive process should be much faster than the contents mixing events that we measure; our contents mixing experiments provide information primarily about the rate of conversion of initial to final intermediate and the rate of conversion of final intermediate to a pore. Figure 2B presents time courses of fusion pore formation (contents mixing) in the presence and absence of 2 mol % perturbants. Contents mixing time courses were described by a single exponential for control, GM1, and LPC vesicles and by a double exponential for hexadecane, DOG, DPhPC, DNPC, DEPC, and GM1 + hexadecane vesicles. The kinetics parameters derived from these time courses are presented in Table 1. The three lipids that failed to produce a second, fast exponential (GM1, LPC16, and LPC24) all have positive intrinsic curvatures. Instead of induction of a fast component, we observed a reduction in the already slow initial rate of contents mixing for all three of these lipids (Table 1). The two LPC species accomplished this by reducing the rate but not the extent of contents mixing, while GM1 reduced both the rate and the extent. However, the effect of GM1 on the extent of contents mixing probably reflects its effect on aggregation, as suggested by its effect on the extent of lipid mixing. All three lipids also produced a reduction in the slower rate constant for lipid transfer between two contacting lipid bilayers (k_2 in Table 1 and Figure 3A inset), which has also been suggested to reflect in part inner leaflet mixing associated with formation of a fusion pore (*6*, *31*, *32*). Thus, these lipids interfere with pore formation.

Table 2: DPH and TMA-DPH Fluorescence Anisotropy for PC/PE/SM/CH (35:30:15:20 mol Ratio) SUVs in the Presence of 2 mol % Perturbants[a]

systems	DPH anisotropy in buffer	DPH anisotropy in 5% PEG	TMA-DPH anisotropy in buffer	TMA-DPH anisotropy in 5% PEG
control	0.164	0.165	0.245	0.253
GM1	0.161	0.170	0.249	0.252
DNPC	0.169	0.170	0.245	0.253
lysoPC (C_{24})	0.163	0.165	0.246	0.255
lysoPC (C_{16})	0.157	0.181	0.240	0.244
hexadecane	0.160	0.164	0.240	0.246
hex/GM1	0.167	0.169	0.250	0.255
DOG	0.163	0.167	0.246	0.250
DPhPC	0.157	0.161	0.241	0.244

[a] Errors in anisotropy values were ±0.005−0.008.

DOG, DPhPC, long chain PCs, and hexadecane dramatically enhanced both the initial rate and extent of contents mixing without much change in leakage (Figure 2B,C). The increase in initial rate was produced by appearance of a second, fast component of contents mixing of smaller magnitude than the slow component seen in the control but roughly an order of magnitude faster (Table 1). The increase in extent of fusion reflects both an increase in the extent of the slow component and the appearance of the fast component. We have reported previously that conditions that stress bilayer packing (e.g., high curvature, fusion peptides, high PEG concentration) promote formation of a fast pore associated with the initial intermediate (*32*, *33*). It appears that even small amounts of lipids with a negative intrinsic curvature have the same effect.

DOG has a very large negative intrinsic curvature, and its effect on contents mixing was much more dramatic than for other lipids. DPhPC also has negative intrinsic curvature. Long chain, unsaturated PCs such as DEPC and DNPC are expected to have a slight negative intrinsic curvature with respect to DOPC (Figure 1). We conclude that all negatively curved lipids promoted pore formation, consistent with the stalk hypothesis. But, can we explain the dramatic effect of long chain lipids solely on the basis of their intrinsic curvature? To answer this question, we first must address what other effects these perturbants might have on bilayer structure and interactions.

Effect of Perturbants on the Acyl Chain and Interface Regions. The fluorescence anisotropies of DPH and TMA-DPH in control vesicles (PC/PE/SM/CH) and in the presence of 2 mol % perturbants in buffer and in 5% PEG are shown in Table 2. These results clearly show that the presence of 2 mol % perturbant molecules had no effect on packing either in the interior or in the interface region of our membranes. We also verified that 4 mol % of long chain lipid (DNPC) and GM1 (data not shown) had no effects. This is consistent with the effects of perturbants on dipalmitoylphosphatidylcholine vesicles that we have reported in an earlier publication (*34*). Thus, changes in fusion promoted by these perturbants are not due to measurable changes in packing either in the interior or at the interface of the bilayer.

Effect of Perturbants on Membrane Phase Behavior. While it is not likely, we felt it best to verify that the lipid perturbants examined do not act by producing phase separations under the conditions of our experiments. We have previously shown that PC/PE/SM/CH vesicles are optimally fusogenic (*23*), and we demonstrated for ourselves by DPH fluorescence anisotropy and differential scanning calorimetry (data not shown) that this lipid mixture does not have a phase transition between 10 and 60 °C. This does not rule out the possibility of liquid-phase inhomogeneity contributing to the fusogenicity of this lipid composition under our experimental temperature, but this is an uncertainty that we accept as the price for working with an optimally fusogenic lipid mixture that mimics the composition of natural fusing membranes (*23*). There was also no indication of phase separation in the presence of the lipid perturbant (GM1) with the most dramatic effects on fusion under our experimental conditions. Thus, there is no reason to invoke inhomogeneous distribution of components over the lamellar phase as an explanation of our results. Naturally, the failure to observe lamellar phase separation cannot rule out the possibility that perturbant molecules could partition either into or out of the region of intervesicle contact where the fusion intermediate forms. Indeed, there is evidence that pyrene-containing probes of different molecular shapes and properties do partition unequally into some region of the fusing complex during the fusion process (*35*).

Effect of Perturbants on Interbilayer Distance. We also asked whether the perturbants that we have used might enhance or retard fusion by altering interbilayer approach. With the kind assistance of Tom McIntosh of Duke University, we obtained lamellar repeat periods of PC/PE/SM/CH (control) and perturbant vesicles, which were the same (64−65 Å) except in the presence of GM1 (71 Å), as expected. The lamellar repeat period contains the width of both the bilayer and the fluid space between adjacent bilayers. Thus, to determine from lamellar repeat distance the width of fluid spaces between bilayers, it is necessary to know the bilayer thickness for the bilayers. Since only 2−3 orders of lamellar diffractions were recorded, it was not possible to calculate electron density profiles to determine bilayer widths. However, it is very unlikely that the very small amount of (2−4 mol %) perturbants used in the present study would change bilayer width. Since the repeat periods were unchanged, we can conclude that the interbilayer distances very likely remain unchanged in the presence of all perturbants except GM1. The large headgroup of GM1 is expected to protrude roughly 18−20 Å above the interface (on the basis of volume arguments), comparable to the phosphate−phosphate water distance (18−22 Å, based on our previous measurements for this lipid mixture; *23*). Thus, we think that the large repeat period observed in the presence of GM1 is due to steric effects on the water space rather than to effects on the bilayer thickness. We conclude that, except for GM1, any effect of perturbants on fusogenicity is not due to effects on interbilayer distance.

Perturbant Intrinsic Curvature and Fusion. Having eliminated other possible influences of perturbants that might affect fusion, we are now in a position to examine whether perturbant intrinsic curvature can explain their effects on fusion. Lipid molecular shape is by convention gauged in terms of the ratio of cross-sectional areas of acyl chain and headgroup (glycerol plus alcohol moieties) regions (*36*). To examine our results in terms of perturbant molecular shape, we needed estimates of the cross-sectional areas of perturbants in the headgroup and acyl-chain regions of the bilayer. The method of Israelachvili (*36*) is often used to estimate the chain cross section of lipid molecules with different chain lengths, but this is based on X-ray data for diacyl-phosphatidylcholines and makes the assumption that the ratio of headgroup and chain areas is one (*37*). Thus, this method is of little use to us in estimating the actual area ratios of different diacyl-phosphatidylcholine molecules. For this reason, we obtained direct experimental estimates of head and chain cross sections of diacyl-phosphatidylcholines from the literature. Petrache et al. (*38*) reported the mean interfacial area for a series of phosphatidylcholines incorporated into multilayers obtained using measured ^2H order parameters. Balgavy et al. (*39*) obtained estimates of the same parameter along with the bilayer thickness for extruded single-lamellar vesicles using small-angle X-ray- and neutron-diffraction data. Both groups found that the area at the interface decreased linearly with increasing carbon atoms in the chain. The hydrocarbon chain length also varied linearly with the number of carbon atoms in the acyl chain (carbon chain C_{10} to C_{18}) (*38*). The volume of the acyl chain region, excluding the carbonyl carbon, was obtained by taking $V_{CH_2} = 30$ Å^3, $V_{CH} = 20.5$ Å^3, and the volume of $CH_3 = 2V_{CH_2}$ (*40*). We then obtained the acyl chain area of different lipid molecules from the ratio of hydrocarbon volume/acyl chain length and obtained the area ratio from the ratio of area at the interface/area of acyl chain region. We estimated the area of DOPC at the interface ($A_w = 77.2$ Å^2) and at the acyl chain region ($A_t = 81.88$ Å^2) based on X-ray scattering results (*41*) to obtain the cross-sectional area ratio (head/chain) of 0.94. This area ratio compares well with the area ratio of 0.96 obtained by the methods outlined above, thus validating our approach.

We estimated the head group and chain areas of dioleolyglycerol (DOG) by linear fits of the change of these areas for DOPC/DOG mixtures with diacylglycerol content (*41*). The cross-sectional area of the GM1 headgroup was taken from Maggio et al. (*42*). The cross-sectional area for GM1 acyl chains was calculated as for the phosphatidylcholine acyl chains. For lyso lipids, we took the headgroup area to be that of phosphatidylcholine, and the acyl chain area was calculated as the ratio of acyl chain volume by length. The cross-sectional areas of DPhPC were obtained from Dr. Huey W. Huang, Department of Physics & Astronomy, Rice University, Houston, Texas. The perturbant area ratios obtained in this way are given in Table 3.

For mixtures of GM1 plus hexadecane, it is more difficult to imagine what the effective area ratio might be. Chen et al. (*43*) showed that, while short chain hydrocarbons intercalate into the hydrocarbon space between the phospholipid chains and change the effective curvature in the H_{II} phase, long chain alkanes such as hexadecane influence more the interstitial region and do not appreciably change the curvature and bending modulus. Thus, hexadecane does not affect significantly the radius of curvature, but it does fill space. For this reason, it seems most reasonable to assign the intrinsic curvature of GM1 to the mixture of GM1 and hexadecane.

Figure 4 shows the effects of 2 mol % perturbants of different molecular shapes on the events associated with

Table 3: Cross-Sectional Areas of Lipid Headgroups and Acyl Chains[a]

systems	acyl chain length (Å)	volume of chain (Å^3)	area of headgroup (Å^2)	area of acyl chain (Å^2)	A_{head}/A_{tail}
DPhPC			65.0[b]	100[b]	0.65[b]
DOPC	14.3	978	65.7	68.4	0.96
DEPC	18.0	1196	62.3	66.4	0.94
DNPC	20.0	1308	60.6	65.4	0.93
lyso(C_{16})	12.4	448	67.4	36.1	1.87
lyso(C_{24})	20.0	672	60.6	33.6	1.80
GM1	13.4	937	170.0[b]	69.9	2.43
DOG			54.0	263	0.207
DiPoPE			50.1	94.9	0.53

[a] Cross-sectional ratio of DiPoPE calculated from DOPE area ratios (*43*). Variation of headgroup and acyl chain length area of DiPoPE was corrected based on PC area (*38*, *39*). All other area ratios obtained as described in text. [b] Data from experiments communicated by Dr. Huang (Department of Physics & Astronomy, Rice University, Houston, Texas).

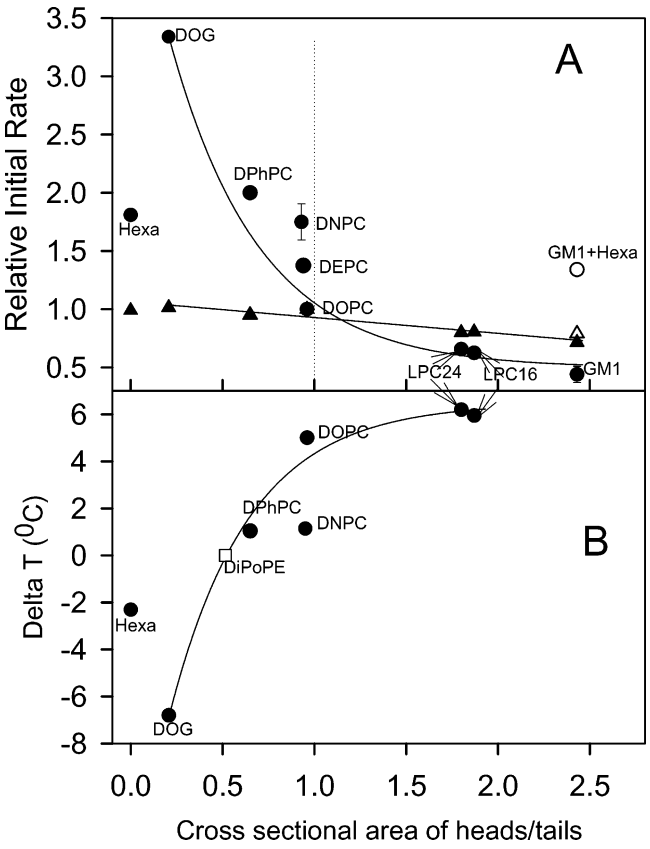

FIGURE 4: (A) Effect of lipid shape on the initial rate of 5 wt % PEG-mediated contents mixing (○) and lipid mixing (▲) between SUVs. Initial rates are shown relative to those of control (no perturbant) SUVs. These relative rates obtained in the presence of 2 mol % perturbant are plotted as a function of the ratio of cross-sectional area of headgroup/acyl chain for different perturbants with the perturbant responsible for each point indicated. The cross-sectional area ratios were determined as described in Results and Discussion. Points are added at area ratio = 0 for hexadecane and at area ratio 2.43 for a mixture of GM1 and hexadecane (open symbols). Panel B shows the effect of 2 mol % of lipid perturbants on the $L_\alpha - H_{II}$ phase transition temperature of DiPoPE (□). The plot shows the difference of temperatures ($T_{DiPoPE} - T_{pert}$) as a function of cross-sectional area ratios (Table 3) of different lipids. Again, labels indicate the perturbant responsible for each point.

PEG-mediated fusion of SUVs presented as a function of the cross-sectional area ratio. For lipids with ratios >1, the initial rates of both lipid mixing (triangles) and contents mixing (circles) decreased mildly with increasing ratio. This suggests that the minimal effect of positively curved perturbants (e.g., GM1, LPC16) on fusion is due primarily to inhibition of formation of the initial intermediate, a process reflected in the initial rates of lipid transfer (i.e., lipid mixing) between fusing vesicles. By contrast, the initial rate of vesicle contents mixing increased dramatically with decreasing ratio below an area ratio of 1, while that of lipid transfer increased only very slightly with decreasing area ratio. From this, we conclude that the shape of negatively curved (ratio < 1) perturbants (e.g., DPhPC, DOG) had a much more dramatic effect on steps of the fusion process leading from the initial intermediate to pore formation than on formation of the initial intermediate of the fusion process.

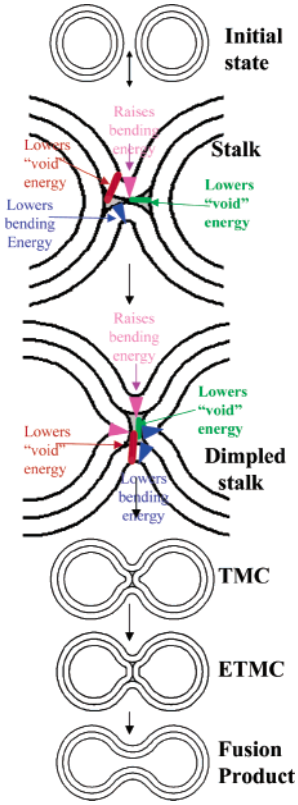

FIGURE 5: Schematic model of the sequence of structures leading to fusion according to the stalk hypothesis (*31*). The initial intermediate (stalk) is thought to form by rearranging the outer leaflets of closely contacting bilayers in a fashion that alters membrane topology away from the normal bilayer morphology. Evolution of the stalk to a trans-monolayer contact (TMC) and to an extended TMC involves rearrangements in nonbilayer structures without a change in membrane topology. The free energy of such nonbilayer lipidic structures is dominated by monolayer bending and hydrophobic mismatch or "void" (illustrated as shaded areas) energies (*60*). Stable fusion pores can form only to the extent that the unfavorable free energy of these intermediates can be overcome by thermal energy. The effects of intrinsically positively curved lipids (purple), long-chain lipids (red), negatively curved lipids (blue), and hexadecane (green) are illustrated.

Effects of Perturbants on the Lamellar−Hexagonal Phase Transition. The initial intermediate of the fusion process is often described in terms of a structure in which contacting monolayers of two abutting membranes join to form a highly curved structure (net negative curvature stress) originally termed a "stalk" (*1*, *44*) (see Figure 5). In this state, lipids are thought to pass freely between the "hemifused" or joined

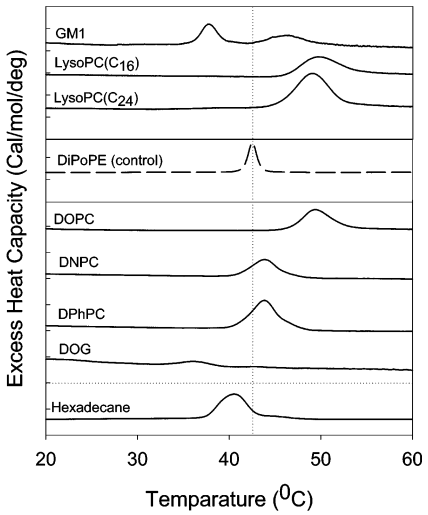

FIGURE 6: Effect of perturbants on the $L_\alpha-H_{II}$ phase transition temperature of DiPoPE (− − −). Shown are plots of excess heat capacity vs temperature of DiPoPE in the presence and absence of 2 mol % of different perturbants with the perturbant leading to each curve indicated next to the curve. The thermograms were recorded at a scan rate of 30 °C/h. The vertical dotted line indicates the $L_\alpha-H_{II}$ phase transition temperature of DiPoPE. Details of experimental conditions and procedures are given in Materials and Methods.

outer monolayers (*5*). The transformation of this structure into a pore at least in some model membranes involves passing through another transiently stable highly curved intermediate (*6*), which we have suggested might be the expanded "trans-monolayer contact" (ETMC) or "septum". Siegel first described in detail the "trans-monolayer contact" (TMC) as a possible structure on the path to fusion (*7*), and we have suggested that it is the transition state for moving from the stalk to the final intermediate (ETMC) (*45*). The free energy of this barrier is determined mainly by monolayer bending energy and the "frustration" energy associated with the inability of smoothly bent monolayers to describe the highly bent shape of the required intermediates (*45*). The frustration energy has been estimated either in terms of the energy of hypothetical "voids" defined by the hydrophobic surfaces of smoothly bent and uniformly packed monolayers (*4*, *45*) or in terms of the energy associated with tilting or splaying acyl chains to fill these spaces (*46*). In either case, it is generally thought that the structures involved in transitioning between the lamellar and hexagonal phases are similar to the transition structures that must be involved in fusion (*4*, *7*). While a number of studies have reported the effects of some of the perturbants examined here on the lamellar-to-hexagonal phase transition (*41*, *43*, *47*), most use very high concentrations of perturbant molecules and do not use a common lipid matrix. For this reason, we examined the effects of a low concentration (2 mol %) of our lipid perturbants on the lamellar to hexagonal phase transition of a common matrix lipid (DiPoPE) so as to compare to their effects on the rates of processes associated with PEG-mediated fusion.

Thermograms showing the effects of perturbants on the DiPoPE $L_\alpha-H_{II}$ phase transition are shown in Figure 6. The $L_\alpha-H_{II}$ phase transition temperature of pure DiPoPE under our experimental conditions was 43 °C, consistent with a report in the literature (*48*). DOG and hexadecane shifted the transition to lower temperature, and all other lipids shifted it to higher temperature with respect to the DiPoPE control. All perturbants except GM1 produced a simple shift in the phase transition temperature. However, we observed two peaks in the presence of 2 mol % GM1. By explanation of this, we suggest that GM1 could promote formation of a cubic phase (Q_{III}) prior to formation of the H_{II} phase. We base this on several reports. First, it has been reported, using X-ray diffraction, that DiPoPE might form Q_{III} phase when incubated for long time at 39 °C, although the formation of this phase was not detected during calorimetric scans at normal scan rates (*48*). Second, the disaccharides sucrose and trehalose accelerate the formation of the cubic phase in PE dispersions (*49*, *50*), and GM1 obviously contains such a polysaccharide group. Finally, GM1 alone did not show a transition, ruling out the possibility that the lower transition seen with GM1 in Figure 6 is due to pure GM1 micelles. Similarly, we did not observe a transition within our experimental temperature range for PC/PE/SM/CH vesicles containing 2 mol % GM1, verifying that GM1 did not separate out to yield a separate melting phase within lamellar structures. Thus, we think that the lower transition seen in Figure 6 for GM1-containing membranes is probably for the $L_\alpha-Q_{III}$ phase transition, while the second and higher transition is probably for either the $L_\alpha-H_{II}$ or $Q_{III}-H_{II}$ phase transition. To distinguish between these two possibilities, we ran the same sample 3−5 times (cycling), leading to the disappearance of the higher temperature peak, suggesting that this is the $L_\alpha-H_{II}$ transition. However, since we cannot be sure of the origin of the higher temperature peak, we cannot reliably measure the effect of GM1 on the $L_\alpha-H_{II}$ phase transition.

The shifts in phase transition temperature for all perturbants except GM1 are plotted as a function of the ratio of headgroup to chain cross-sectional areas in Figure 4B. The phase transition shifts for most of the perturbants (including the zero shift for the control DiPoPE data) seem to fall on a smooth, roughly hyperbolic curve with compounds with ratios >0.53 (the cross-sectional ratio of DiPoPE) shifting the transition to higher temperature and DOG and those with a ratio of <0.21 shifting the transition to lower temperature. The same approximately hyperbolic behavior is seen in the variation of the initial rate of contents mixing with cross-sectional ratio (Figure 4A). The variation of L_a-H_{II} phase transition temperature with lipid composition is thought to be mainly due to the effect of lipid curvature on the relative stabilities of the lamellar and hexagonal phases (*4*). Thus, the parallel between the variation with cross-sectional area ratio of phase transition shift (Figure 4B) and of initial rate of fusion (Figure 4A) suggests that the curvature of perturbants also dominates their effects on the free energy of whatever fusion intermediate(s) limit conversion of the initial stalk to a final fusion pore. However, the fact that data for some perturbants (long-chain lipids) did not fall on a smooth curve indicates that a property of these perturbants other than curvature has a significant influence on both fusion pore formation and the equilibrium between lamellar and hexagonal phases.

Non-Curvature-Related Effects. The effects of long chain lipids (DNPC and DEPC) do not fall on the smooth curve defined by the effects of other perturbants in Figure 4A. Rather, these two lipids promoted fusion pore formation

much more than would be predicted on the basis of their cross-sectional area ratios (i.e., they fall above the line defined by the majority of perturbants). In contrast to their anomalous effects on fusion pore formation, these long-chain lipids affected lipid transfer just like other lipids with similar area ratios. Why do long chain lipids show this anomalous effect on fusion pore formation?

Our hypothesis to explain the unusual effects of long chain lipids is that long acyl chains not only create slight negative intrinsic curvature (with respect to DOPC) but also provide mass near the center of the bilayer that can lower the "void" free energy. This is based on the observation that these two lipids had an effect comparable to the effect of hexadecane on the initial rate of fusion (points at volume ratio = 0 in Figure 4A). DNPC and hexadecane also share the property of stabilizing the hexagonal phase. While DNPC would be expected to stabilize hexagonal phase on the basis of its intrinsic curvature, it did so much more dramatically than did DOPC, which has nearly the same area ratio (compare the points for DOPC and DNPC in Figure 4B). Of course, hexadecane is not an amphipathic lipid and thus does not have an intrinsic curvature, which is why the results for this perturbant are shown at ratio = 0. Hexadecane has been shown to stabilize nonlamellar structures in hexagonal phases, probably by reducing the "frustration" or "void" free energy (*51*). It is also observed to promote fusion (*22*, *52*, *53*), probably by the same means. Since the "void" free energy is a major contributor to the free energy barrier between the initial stalk intermediate and the TMC intermediate, lowering it by even a small amount has a dramatic effect on the barrier height (*45*). Thus, it seems that both hexadecane and long chain lipids produce an increased rate of contents mixing based on their ability to fill space in the hydrophobic region of the bilayer and thus lower "void" free energy.

To test this idea further, we examined the effect of a "void"-filling agent (hexadecane) on the fusion inhibitory effect of a highly positively curved lipid (GM1). The rationale for this experiment was that hexadecane should affect the "void" energy and not the curvature energy of intermediates and thus should show an effect in the presence of GM1 comparable to its effect in its absence. Figure 2 shows the kinetic data (deep green plot) that led to the initial rates of lipid mixing (open triangle) and contents mixing (open circle) plotted in Figure 4A at the cross-sectional ratio of GM1 (2.46). These are plotted at this cross-sectional ratio since hexadecane should not contribute to the cross-sectional ratio; it should only fill volume. Consistent with our prediction, hexadecane promoted fusion in the presence of GM1 to about the same extent (compare open and filled circles at ratio = 2.43) that it promoted fusion of our matrix lipid mixture (see closed circle at ratio = 0). These changes in fusion rate correspond to reductions in the fusion activation free energy of roughly 0.74 and 0.71 kT, respectively. In contrast to its effect on fusion, hexadecane could not overcome GM1's inhibition of the rate of lipid mixing. This is seen by comparing the open and filled triangles at ratio = 2.46 in Figure 4A. This is consistent with the fact that it did not influence at all the rate of lipid mixing when used alone in our matrix lipid mixture (triangle at ratio = 0 in Figure 4A). Thus, hexadecane clearly acted by a mechanism distinct from and, in the case of contents mixing, additive to that of molecular curvature. The rate of fusion in the presence of DNPC and DEPC relative to the rate in the presence of DOPC (a lipid with nearly identical intrinsic curvature) suggested lowering of the activation free energy by about 0.67 and 0.39 kT, respectively, indicating that these two lipids also lowered the activation energy by an amount comparable to hexadecane and also by a mechanism independent of curvature. It is reasonable to conclude that the ability of hexadecane or long chain lipids to lower "void" energy must be counted along with their ability to alter bending energy in considering their effects on fusion.

Perturbant Location. To this point, our comments have ignored the issue of where in the fusing vesicle the perturbants might be located. These molecules are not expected to distribute equally between the outer and inner leaflets of highly curved SUVs but may distribute either toward the leaflet that best accommodates their intrinsic curvature or, at the very low concentrations that we have used, to the outer leaflet, probably because small numbers of perturbant molecules can be most easily accommodated in regions of reduced packing density (*54*, *55*). In addition, perturbant molecules may distribute unequally between the lamellar and nonlamellar or hemifused portions of the vesicles (*35*). The intrinsic curvature for the fusogenic lipid mixture DOPC/DOPE/SM/CH (35:30:15:20) used for our studies can be calculated as -27 nm^{-1} based on the assumptions that the net curvature was a mole-fraction-weighted sum of component curvatures and that the intrinsic curvature of SM is that of dipalmitoylphosphatidylcholine (*45*, *56*). Addition of 2 mol % perturbants to this mixture will not appreciably change its average intrinsic curvature. Thus, the effects that we see must reflect the effects of perturbants on the local regions where lipids are rearranging. This implies that the lipid perturbants partition into regions of local lipid rearrangement to produce larger effects than one would predict from their effect on mean bilayer curvature. Of course, we have no way to know the details of perturbant partitioning during the fusion process or during conversion of the lamellar to the hexagonal phase. However, we do know that, no matter how strong may be the packing (i.e., enthalpic) driving force for unequal partitioning, entropic considerations will oppose extremes of unequal partitioning, especially for the low perturbant concentrations that we are using. Thus, our perturbants will affect packing in all of the different regions of the fusing SUVs that we studied, although we cannot know the exact extent of their effects on different regions.

The Stalk Model of Fusion. Inhibition of the extent of fusion by positively curved lipids such as LPC_{16} has previously been offered as support for the stalk hypothesis, since these lipids should raise the free energy of the strongly negatively curved fused monolayers of the stalk (see Figure 5) (*5*, *12*). We have also noted that positively curved lipids incorporated into contacting leaflets might also inhibit fusion by lowering the free energy of the unfused SUVs (*17*). Conversely, it has also been pointed out that positively curved lipids inserted into the noncontacting or trans monolayers might promote fusion by conforming to the shape of these monolayers in the initial fusion pore (*5*). Of course, perturbants that alter the free energies of intermediate states such as the stalk or initial fusion pore can be expected to alter only the rate of fusion, not necessarily the extent of fusion,

as is most often reported. In addition, perturbing lipids present in our experiments at very low concentrations in the bilayer should partition into both leaflets and, as noted above, in this way affect the free energies of different intermediates differently. Thus, one could argue that positively curved perturbants might increase or decrease the rate of fusion, depending on the extent to which they might stabilize the initial fusion pore (increased rate), destabilize the initial state (lowered rate), or lower the free energy of the stalk intermediate (increased rate). However, because we have focused on *rates* of lipid and contents mixing, we can make some distinctions among these various possibilities.

First, the failure of lipids of different curvature to have a significant effect on the initial rate of lipid mixing indicates that lipid shape has little effect on the transition state leading to formation of the first intermediate (stalk). This contradicts our earlier suggestion that positively curved lipids such as LPC_{16} might inhibit fusion by stabilizing the unfused state and therefore inhibiting formation of the initial intermediate (*17*). Second, since perturbants did alter the rate of fusion, they must change the free energies of one or more structures intermediate between the initial stalk and the fusion pore. A calculation of the free energy profile for conversion of the stalk to a slightly expanded TMC shows two free energy minima separated by a free energy barrier (*45*), consistent with the experimental reports that at least two intermediate "states" (slightly expanded stalk and ETMC in Figure 5) exist on the path to fusion pore formation between highly curved vesicles (*6*, *32*). The free energy barrier between intermediate states exists at roughly the geometry of the TMC (*45*). We presume that a second free energy barrier exists between the ETMC intermediate and the initial fusion pore and that a third may exist between the initial pore and the final, stable pore. In the highly curved vesicles that we have studied, it is likely that any initial pore that might form would rapidly convert either to the intermediate from which it derived or to a stable fusion pore. Thus, we assume that the rate of initial pore formation to a stable pore would not limit the rate of fusion and focus our discussion on the TMC barrier and the barrier between the ETMC and pore. If our results are consistent with the expected effects of lipid perturbants on one or both of these barriers, we would conclude that they support the stalk hypothesis for fusion.

The bending energy is maximal at the TMC, so this barrier is lowered by increasingly negative intrinsic curvature (*45*). In the TMC, both the cis and trans monolayers experience negative curvature stress (Figure 5), and positively curved lipids (LPC_{16}, LPC_{24}, GM1) will therefore raise the free energy of this intermediate and lower the rate of fusion, as we observe (Figure 4A). Conversely, negatively curved lipids (DPhPC, DOG) will lower the free energy of this barrier and increase the rate of fusion, also as we observe (Figure 4A). In addition to curvature free energy, the most significant contribution to the free energy of the TMC is the "void" energy (*45*). Perturbants that can fill space near the center of the bilayer (DEPC, DNPC, hexadecane) will lower the "void" energy and thus significantly promote fusion, also as we have observed (Figure 4A).

It could also be that perturbants lower the activation energy for conversion of the extended TMC to a pore. Pore formation is topologically analogous to stalk formation from contacting membranes and, if contacting membranes are sufficiently highly curved, molecular dynamics simulations of a cubic-hexagonal transition suggest that the two processes are really the same process occurring in opposite directions (*57*). Since the rate of formation of the initial intermediate was fairly independent of perturbant curvature, we do not expect the rate of pore formation to be much affected by perturbants either. Thus, we suggest that the effect of increasing negative perturbant intrinsic curvature is to lower the barrier between the initial and second intermediate, which then can degrade to a pore.

Thus, our results, which detail the influence of lipid perturbants on the kinetics of lipid rearrangements during fusion between curved vesicles, can be interpreted in terms of the energetics of the intermediates proposed by the stalk hypothesis (*45*). The agreement of our results with predictions based on this interpretation provides significant support for the validity of the stalk hypothesis. Clearly, the structures that exist on the path to fusion are dynamic and less well defined than suggested by Figure 5, but our results support a model like that shown. Further, they suggest that not only the bending energy but also the "void" energy provide significant barriers to fusion. The role of fusion protein machines need not simply be that of altering either the intrinsic (*58*) or mechanical (*59*) curvature of a lipidic fusion intermediate but could also be that of "filling void", that is, promoting the formation of a transitory nonlamellar packing state, such as that described by Bentz (*10*).

ACKNOWLEDGMENT

We thank Dr. Thomas J. McIntosh, Department of Cell Biology, Duke University Medical Center, Durham, NC, for help with measurements of lamellar repeat distances by X-ray scattering. We thank Dr. Huey W. Huang, Department of Physics and Astronomy, Rice University, Houston, Texas, for providing us the cross-sectional area of headgroup and acyl chain of DPhPC. Finally, we thank three reviewers for many useful suggestions that helped us to improve and sharpen our arguments considerably.

REFERENCES

1. Markin, V. S., Kozlov, M. M., and Borovjagin, V. L. (1984) *Gen. Physiol. Biophys. 3*, 361−377.
2. Leikin, S. L., Kozlov, M. M., Chernomordik, L. V., Markin, V. S., and Chizmadzhev, Y. A. (1987) *J. Theor. Biol. 129*, 411−425.
3. Kozlov, M. M., Leikin, S. L., Chernomordik, L. V., Markin, V. S., and Chizmadzhev, Y. A. (1989) *Eur. Biophys. J. 17*, 121−129.
4. Siegel, D. P. (1993) *Biophys. J. 65*, 2124−2140.
5. Chernomordik, L., Chanturiya, A., Green, J., and Zimmerberg, J. (1995) *Biophys. J. 69*, 922−929.
6. Lee, J., and Lentz, B. R. (1997) *Biochemistry 36*, 6251−6259.
7. Siegel, D. P. (1999) *Biophys. J. 76*, 291−313.
8. Chernomordik, L. V., and Zimmerberg, J. (1995) *Curr. Opin. Struct. Biol. 5*, 541−547.
9. Lentz, B. R., Malinin, V., Haque, M. E., and Evans, K. (2000) *Curr. Opin. Struct. Biol. 10*, 607−615.
10. Bentz, J. (2000) *Biophys. J. 78*, 886−900.
11. Bonnafous, P., and Stegmann, T. (2000) *J. Biol. Chem. 275*, 6160−6166.
12. Chernomordik, L. V., Vogel, S. S., Sokoloff, A., Onaran, H. O., Leikina, E. A., and Zimmerberg, J. (1993) *FEBS Lett. 318*, 71−76.
13. Chernomordik, L., Kozlov, M. M., and Zimmerberg, J. (1995) *J. Membr. Biol. 146*, 1−14.
14. Chernomordik, L., Leikina, E., Cho, M. S., and Zimmerberg, J. (1995) *J. Virol. 69*, 3049−3058.

15. Vogel, S. S., Leikina, E. A., and Chernomordik, L. V. (1993) *J. Biol. Chem. 268*, 25764−25768.
16. Chernomordik, L. V., Leikina, E., Frolov, V., Bronk, P., and Zimmerberg, J. (1997) *J. Cell Biol. 136*, 81−93.
17. Wu, H., Zheng, L., and Lentz, B. R. (1996) *Biochemistry 35*, 12602−12611.
18. Lee, J., and Lentz, B. R. (1997) *Biochemistry 36*, 421−431.
19. Martin, I., Dubois, M. C., Saermark, T., Epand, R. M., and Ruysschaert, J. M. (1993) *FEBS Lett. 333*, 325−330.
20. Pecheur, E. I., Martin, I., Bienvenue, A., Ruysschaert, J. M., and Hoekstra, D. (2000) *J. Biol. Chem. 275*, 3936−3942.
21. Lentz, B. R., and Lee, J. K. (1999) *Mol. Membr. Biol. 16*, 279−296.
22. Malinin, V. S., Frederik, P., and Lentz, B. R. (2002) *Biophys. J. 82*, 2090−2100.
23. Haque, M. E., McIntosh, T. J., and Lentz, B. R. (2001) *Biochemistry 40*, 4340−4348.
24. Chen, P. S., Jr., Toribara, T. Y., and Warner, H. (1956) *Anal. Chem. 28*, 1756−1758.
25. Schwenk, E., and Werthessen, N. T. (1952) *Arch. Biochem. Biophys. 40*, 334−341.
26. Lentz, B. R., McIntyre, G. F., Parks, D. J., Yates, J. C., and Massenburg, D. (1992) *Biochemistry 31*, 2643−2653.
27. Wilschut, J., Duzgunes, N., Fraley, R., and Papahadjopoulos, D. (1980) *Biochemistry 19*, 6011−6021.
28. Malinin, V. S., Haque, M. E., and Lentz, B. R. (2001) *Biochemistry 40*, 8292−8299.
29. Wu, J. R., and Lentz, B. R. (1991) *Biochemistry 30*, 6780−6787.
30. Wu, J. R., and Lentz, B. R. (1994) *J. Fluoresc. 4*, 153−163.
31. Lee, J., and Lentz, B. R. (1998) *Proc. Natl. Acad. Sci. U.S.A. 95*, 9274−9279.
32. Evans, K. O., and Lentz, B. R. (2002) *Biochemistry 41*, 1241−1249.
33. Haque, M. E., and Lentz, B. R. (2002) *Biochemistry 41*, 10866−10876.
34. Lentz, B. R., Wu, J. R., Zheng, L., and Prevratil, J. (1996) *Biophys. J. 71*, 3302−3310.
35. Malinin, V. S., and Lentz, B. R. (2002) *Biochemistry 41*, 5913−5919.
36. Israelachvili, I. N., Mitchell, D. J., and Ninharm, B. W. (1976) *Chem. Soc., Faraday Trans II*, 1525−1568.
37. Tanford, C. (1972) *J. Phys. Chem. 76*, 3020−3024.
38. Petrache, H. I., Dodd, S. W., and Brown, M. F. (2000) *Biophys. J. 79*, 3172−3192.
39. Balgavy, P., Dubnickova, M., Kucerka, N., Kiselev, M. A., Yaradaikin, S. P., and Uhrikova, D. (2001) *Biochim. Biophys. Acta 1512*, 40−52.
40. Thurmond, R. L., Lindblom, G., and Brown, M. F. (1993) *Biochemistry 32*, 5394−5410.
41. Szule, J. A., Fuller, N. L., and Rand, R. P. (2002) *Biophys. J. 83*, 977−984.
42. Maggio, B., Ariga, T., Sturtevant, J. M., and Yu, R. K. (1985) *Biochemistry 24*, 1084−1092.
43. Chen, Z., and Rand, R. P. (1998) *Biophys. J. 74*, 944−952.
44. Chernomordik, L., Kozlov, M., Melikyan, G., Agidor, I., Markin, V., and Chizmadzhev, Y. (1985) *Biochim. Biophys. Acta 812*, 643−655.
45. Malinin, V., and Lentz, B. R. (2004) *Biophys. J.*, in press.
46. Hamm, M., and Kozlov, M. M. (1998) *Eur, Phys. J. B 6*, 519−528.
47. Fuller, N., and Rand, R. P. (2001) *Biophys. J. 81*, 243−254.
48. Siegel, D. P., and Epand, R. M. (1997) *Biophys. J. 73*, 3089−3111.
49. Rappolt, M., Hickel, A., Bringezu, F., and Lohner, K. (2003) *Biophys. J. 84*, 3111−3122.
50. Tenchov, B., Koynova, R., and Rapp, G. (1998) *Biophys. J. 75*, 853−866.
51. Rand, R. P., Fuller, N. L., Gruner, S. M., and Parsegian, V. A. (1990) *Biochemistry 29*, 76−87.
52. Walter, A., Yeagle, P. L., and Siegel, D. P. (1994) *Biophys. J. 66*, 366−376.
53. Basanez, G., Goni, F. M., and Alonso, A. (1998) *Biochemistry 37*, 3901−3908.
54. Lentz, B. R., and Litman, B. J. (1978) *Biochemistry 17*, 5537−5543.
55. Lentz, B. R., Alford, D. R., and Dombrose, F. A. (1980) *Biochemistry 19*, 2555−2559.
56. Chernomordik, L. V., and Kozlov, M. M. (2003) *Annu. Rev. Biochem. 72*, 175−207.
57. Marrink, S. J., and Tieleman, D. P. (2002) *Biophys. J. 83*, 2386−2392.
58. Colotto, A., and Epand, R. M. (1997) *Biochemistry 36*, 7644−7651.
59. Kozlov, M. M., and Chernomordik, L. V. (1998) *Biophys. J. 75*, 1384−1396.
60. Siegel, D. P. (1993) in *Viral Fusion Mechanisms* (Bentz, J., Ed.) pp 475−512, CRC Press, Inc., Boca Raton, FL.

BI035794J